Available online at www.sciencedirect.com
ScienceDirect
Deep-Sea Research I 54 (2007) 710–731
DEEP-SEA RESEARCH PART I
www.elsevier.com/locate/dsri

Hydrography of chromophoric dissolved organic matter in the North Atlantic

Norman B. Nelson[a,*], David A. Siegel[a,b], Craig. A. Carlson[a,c], Chantal Swan[a], William M. Smethie Jr[d], Samar Khatiwala[d]

[a]*Institute for Computational Earth System Science, Mail Code 3060, University of California, Santa Barbara, CA 93106, USA*
[b]*Department of Geography, University of California, Santa Barbara, CA 93106, USA*
[c]*Department of Ecology, Evolution, and Marine Biology, University of California, Santa Barbara, CA 93106, USA*
[d]*Lamont-Doherty Earth Observatory of Columbia University, Palisades, NY, USA*

Received 20 July 2006; received in revised form 10 February 2007; accepted 19 February 2007
Available online 7 March 2007

Abstract

The distribution and optical absorption characteristics of chromophoric dissolved organic matter (CDOM) were systematically investigated along three meridional transects in the North Atlantic Ocean and Caribbean Sea conducted as part of the 2003 US CLIVAR/CO_2 Repeat Hydrography survey. Hydrographic transects covered in aggregate a latitudinal range of 5° to 62° north along longitudes 20°W (line A16N, Leg 1), 52°W (A20), and 66°W (A22). Absorption spectra of filtered seawater samples were collected and analyzed for depths ranging from the surface to ~6000 m, sampling all the ocean water masses in the western basin of the subtropical North Atlantic and several stations on the North and South American continental slopes. The lowest surface abundances of CDOM ($< 0.1\,m^{-1}$ absorption coefficient at 325 nm) were found in the central subtropical gyres while the highest surface abundances ($\sim 0.7\,m^{-1}$) were found along the continental shelves and within the subpolar gyre, confirming recent satellite-based assessments of surface CDOM distribution. Within the ocean interior, CDOM abundances were relatively high ($0.1–0.2\,m^{-1}$ absorption coefficient at 325 nm) except in the subtropical mode water, where a local minimum exists due to the subduction of low CDOM surface waters during mode water formation. In the subthermocline water masses of the western basin, changes in CDOM abundance are not correlated with increasing ventilation age as assessed using chlorofluorocarbon (CFC) concentrations and the atmospheric CFC history. But dissolved organic carbon (DOC) mass-specific absorption coefficients of CDOM increase with increasing ventilation age in the deep sea, indicating that CDOM is a refractory component of the DOC pool. The overall CDOM distribution in the North Atlantic reflects the rapid advection and mixing processes of the basin and demonstrates that remineralization in the ocean interior is not a significant sink for CDOM. This supports the potential of CDOM as a tracer of ocean circulation processes for subducted water masses.

Keywords: CDOM; North Atlantic; Water masses; Tracers; Diagenesis

1. Introduction

The chromophoric fraction of dissolved organic matter (CDOM) is ubiquitous in all natural waters

*Corresponding author. Tel.: +1 805 893 3202; fax: +1 805 893 2578.
E-mail address: norm@icess.ucsb.edu (N.B. Nelson).

0967-0637/$ - see front matter © 2007 Elsevier Ltd. All rights reserved.
doi:10.1016/j.dsr.2007.02.006

(e.g., Kalle, 1938; Jerlov, 1953; Siegel et al., 2002). CDOM is operationally defined using the absorption coefficient of the material that passes 0.2 μm filters and is often quantified as the optical absorption coefficient (m^{-1}) at a selected wavelength, such as 325 nm (Nelson and Siegel, 2002). The absorption spectrum of CDOM in natural waters increases exponentially with decreasing wavelength, a characteristic of the absorption spectrum that allows it to be distinguished from the other predominant light absorbing materials in the water column phytoplankton pigments (e.g., Siegel and Michaels, 1996; Nelson et al., 1998). This in turn allows the global surface distribution of CDOM to be assessed from space by ocean color sensors (Siegel et al., 2002). CDOM regulates the penetration of UV light into the ocean and mediates photochemical reactions, therefore playing an important role in many biogeochemical processes in the surface ocean including primary productivity and the air–sea exchange of radiatively important trace gases (e.g., Mopper et al., 1991; Arrigo and Brown, 1996; Zepp et al., 1998; Toole and Siegel, 2004). CDOM is also of interest as a component of the dissolved organic matter (DOM) pool, which represents a significant ocean carbon reservoir (e.g., Hansell, 2002). Understanding the dynamics of CDOM in oceanic waters may assist in our understanding of the dynamics of the overall DOM pool, including its photoremineralization and diagenesis.

It is well known that the abundance and distribution of CDOM for many coastal systems is dominated by terrestrial inputs from rivers and runoff, as decomposition of terrestrial organic matter yields light-absorbing compounds such as humic and fulvic acids (Kalle, 1938; Højerslev, 1982; Carder et al., 1989; Del Vecchio and Blough, 2004). Recent work has shown that the open ocean has its own autochthonous sources and sinks (e.g., Nelson et al., 1998; Nelson and Siegel, 2002; Siegel et al., 2002; Steinberg et al., 2004; Yamashita and Tanoue, 2004). In particular, CDOM is produced in the open ocean as a result of heterotrophic processes near the surface (Nelson et al., 1998; 2004; Steinberg et al., 2004; Yamashita and Tanoue, 2004) and is destroyed by solar bleaching in stratified surface waters, Chen and Bada, 1992; Determann et al., 1996; Vodacek et al., 1997; Nelson et al., 1998, 2004; Siegel et al., 2002, 2005a; Del Vecchio and Blough 2004). These local sources and sinks are sufficient to account for seasonal cycles in surface CDOM observed in satellite data by Siegel et al. (2002). The optical activity of CDOM is (almost) never completely eliminated by solar bleaching or other natural processes, suggesting a pool of CDOM that is at least partially resistant to solar bleaching and microbial degradation. It is logical to assume that this material has been carried into the intermediate and deep waters by convective processes and may act as a tracer of ocean circulation and of diagenetic transformations of DOC.

CDOM has been detected in the deep ocean (> 1000 m) by fluorescence methods (Chen and Bada, 1992; Determann et al., 1996) and by absorption spectroscopy from samples collected at Bermuda Atlantic Time-series Study (BATS) site in the northwestern Sargasso Sea (Nelson, unpublished data). The "oceanographic" distribution of CDOM in BATS profiles and in global ocean color imagery (Nelson et al., 1998; Siegel et al., 2002, 2005a, b) suggests that CDOM is transported by large-scale hydrographic processes such as the upwelling and subduction of water masses, as has also been suggested by other field studies (Coble et al., 1998). Thus, CDOM shows potential as a semi-conservative oceanographic tracer that can be bounded at the surface by remote sensing and measured in situ using autonomous sensor systems. This distinguishes CDOM from other oceanographic tracers that must be quantified, even at the surface, by analysis of discrete water samples.

The overall goal of our study is to test the hypothesis that CDOM can act as a semi-conservative tracer. Our main approach is to describe the global distribution of CDOM in the major ocean basins in conjunction with hydrography and other established tracers. This work covers much of the North Atlantic on meridional sections conducted in concert with the US CLIVAR/CO_2 Repeat Hydrography section program ⟨http://ushydro.ucsd.edu/⟩. Here, we describe the distribution of CDOM in surface waters of the North Atlantic and its principal intermediate and deep water masses, and assess this distribution in the context of hydrographic properties, chlorofluorocarbon (CFC) tracers, and optical properties of the CDOM itself. We find patterns and concentrations of CDOM in surface waters are consistent with their assessment from satellite ocean color imagery. Within the oceanic interior, we find that water mass ventilation processes regulate CDOM concentrations in a consistent manner throughout the North Atlantic. In all, this is the first consistent hydrographic survey of CDOM absorption conducted

in the open sea and provides new insights for CDOM cycling and for the cycling of organic matter in general.

2. Methods and data

2.1. Hydrographic data

CDOM observations were made in concert with hydrographic measurements on three transects (Fig. 1) covering a latitude range of 5°N to 62°N along longitudes of 20°W (line A16N, Leg 1), 52°W (line A20), and 66°W (line A22). Hydrographic data were taken with a nominal station spacing of every 50 km. CTD and 36 place bottle trips were spread throughout the entire water column (Feely et al., 2005). Hydrographic parameters sampled include temperature, salinity, dissolved oxygen, primary nutrients (NO_3, PO_4 and SiO_4), inorganic carbon concentrations (nominally pCO_2 and DIC), CFC species (CFC-11, CFC-12 and CFC-113) and dissolved organic carbon (DOC) concentrations. WOCE standard protocols are used for all hydrographic measurements. Details of the measurements protocols, cruise narratives and data sets are available at the Repeat Hydrography Program website ⟨http://ushydro.ucsd.edu/⟩. Computations of neutral density, potential vorticity (PV), partial pressure of CFC-12 (pCFC-12), and AOU were performed using Ocean Data View (Schlitzer, 2004).

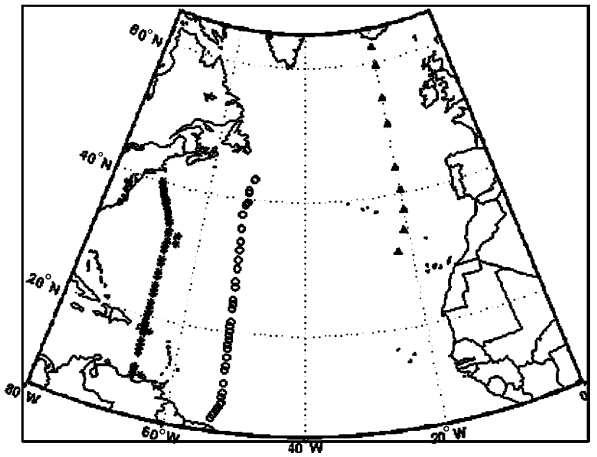

Fig. 1. Distribution of data collected as part of the present study. Symbols indicate stations where CDOM data was collected at the surface. The symbols used for the A16N line (▲), the A20 line (○) and the A22 line (*) are used in the Figs. 3, 4, 6, and 8 to denote the section on which individual samples were taken.

2.2. Water mass definitions

For the purpose of analyzing the distribution of CDOM by water mass in the North Atlantic we have adopted the definitions of Joyce et al. (2001) based upon neutral density (γ^n) isopycnals. We have condensed several of the layers to simplify the statistical analyses (Table 1). Surface waters (SURF) are all waters with neutral density anomalies less than 25 kg m^{-3}. For the seasonal thermocline and subtropical underwater, we have condensed layers 2–4 of Joyce et al. (γ^n range from 25 to 26.4 kg m^{-3}), and are calling this the upper thermocline (UTCL). For the Antarctic intermediate waters (AAIW) we consider two water masses, corresponding to layer 6 of Joyce et al. (γ^n range 27–27.5 kg m^{-3}, which we designate upper (u) AAIW) and layers 7 and 8 together (γ^n range 27.5–27.8 kg m^{-3}, which we designate lower (l) AAIW). For the North Atlantic Deep Water (NADW) we consider the Upper Labrador Sea Water (ULSW, layer 10 of Joyce et al., γ^n from 27.8 to 27.875 kg m^{-3}) and Labrador Sea Water (LSW, layers 11 and 12 of Joyce et al., γ^n from 27.875 to 27.975 kg m^{-3}) as one layer which we designate LSW. We consider two overflow water (OW) components of the NADW, Iceland–Scotland OW (ISOW), γ^n from 27.975 to 28.05 kg m^{-3}, and Denmark Strait OW (DSOW), 28.05–28.14 kg m^{-3}. Antarctic Bottom Water (AABW) is considered to be all water with neutral density greater than 28.14 kg m^{-3}.

2.3. CDOM absorption data

Water samples were prepared for spectrophotometric analysis according to established methods (Nelson et al., 1998, 2004). Samples were drawn from Niskin bottles into acid-washed and Milli-Q (Millipore) rinsed amber glass vials with Teflon liner caps. The samples were then subjected to filtration using 0.2 μm Nuclepore membrane filters that were preconditioned by extraction with Milli-Q water to remove any possible absorbing contaminants. On the A16N line, the samples were kept refrigerated (not frozen) and shipped on ice to UCSB for subsequent analysis (within 4 weeks). We have found that CDOM samples from the open ocean (i.e. with low concentrations of CDOM) prepared in this way remain stable, with repeatable absorbance spectra, for months (Nelson et al., 2004, Nelson and Swan, unpublished data). On the A20 and A22 lines samples were analyzed at sea, usually within 2 h of collection and filtration.

Table 1
Water mass layer definitions in terms of neutral density intervals (based on Joyce et al., 2001) and estimated CFC-12 saturation at formation (this study)

Layer	Abbreviation	γ^n range (kg m^{-3})	CFC-12 saturation (%)
Surface	SURF	18.00–25.00	100[a]
Upper thermocline	UTCL	25.00–26.40	100[a]
Subtropical mode water	STMW	26.40–26.60	94[b]
Lower thermocline	LTCL	26.6–27.00	90[c]
Upper Antarctic intermediate water	uAAIW	27.00–27.50	70[d]
Lower Antarctic intermediate water	lAAIW	27.50–27.80	70[d]
Labrador Sea water	LSW	27.80–27.975	70[e]
Iceland–Scotland overflow water	ISOW	27.975–28.05	43[f]
Denmark Strait overflow water	DSOW	28.05–28.14	75[g]
Antarctic bottom water	AABW	28.14–29.00	70[h]

[a]Most surface and near surface water is within a few percent of saturation with the atmosphere.
[b]Calculated from CFC data measured during the WOCE North Atlantic survey in 1997 along 66°W in the region of STMW formation just south of the Gulf Stream.
[c]Average for 26.6 neutral density surface between the southern edge of the Gulf Stream and 35°N along 52°W measured on the A20 repeat line in 2003.
[d]Rough assumption based on CFC measurements near 50°S made during the WOCE program.
[e]Labrador Sea water defined by this range of neutral density includes upper LSW and classical LSW and the saturation for these two water masses ranges between 60% and 85%, with higher saturations in recent years (Wallace and Lazier, 1988; Pickart et al., 1996; Rhein et al., 1992). A value of 70% was assumed and represents an approximate average between the mid-1980s and late 1990s.
[f]ISOW originates from a poorly ventilated layer in the Nordic Seas and winter mixed layer water it entrains at its point of entry to the Northeastern Atlantic Ocean. The CFC concentration in the resulting mixture has been estimated by Smethie and Fine (2001) and the saturation was estimated from this concentration.
[g]Upper value estimated by Smethie et al. (2000).
[h]Average CFC-12 saturation along the front of the Ross Ice Shelf between 1984 and 2000 (Smethie and Jacobs, 2005).

Spectrophotometric analysis was performed using the UltraPath 200 cm liquid waveguide cell (World Precision Instruments, Sarasota, FL, USA; Miller et al., 2002) and the TIDAS-2 diode array spectrometer (J&M GmbH, FRG). This is a single beam spectrophotometer, so assessment of absorbance of a sample requires two scans: one of a cell filled with blank solution (Milli-Q) and one of the sample itself. The liquid waveguide absorption cell has several advantages over conventional spectrophotometers using 10 cm cuvettes. Sample volumes are smaller (ca. 15 ml) and analysis of an individual sample is rapid ($<$ 2 min/sample), allowing us to analyze many more samples than is practical with a conventional spectrophotometer. Also, the 200 cm path can allow for greater sensitivity, allowing us to better estimate absorption coefficients for low CDOM open ocean surface waters (Nelson and Siegel 2002). The single-beam design of the instrument and the optical characteristics of the waveguide limit the accuracy and precision of the instrument below what would be suggested by the pathlength and the photometric accuracy of the spectrometer. This has some implications that we will now describe.

The liquid waveguide cell has transmission properties that vary with seawater refractive index (D'Sa et al., 1999; Byrne and Kaltenbacher, 2001; Miller et al., 2002). Higher refractive index solutions such as seawater transmit more photons through the waveguide than pure water, leading to an apparent optical absorbance less than zero at certain wavelengths. The established procedure for correcting this refractive index effect is to prepare a blank sodium chloride solution with a similar refractive index to the sample, using a refractometer (Miller et al., 2002). This procedure was impractical for our purpose because of the large number of samples to be collected and analyzed, so an empirical method for correction was developed. This takes advantage of the fact that salinity is the main factor controlling the refractive index of seawater as temperature effects are eliminated by allowing samples to equilibrate before analysis. High-quality salinity measurements were available for each sample bottle collected.

Artificial seawater medium (ASW) was prepared using HPLC-grade Optima^{TM} water, precombusted (450°C) $MgSO_4$, NaCl, KBr, KCl, $CaCl_2$, non-combusted $MgCl_2$ and sterile-filtered $NaHCO_3$.

This basal solution contained most of the diversity of ions and their proportions found in natural seawater (Goldman and McCarthy 1978; McLachlan 1964). A range of ASW salinities was acquired through dilution and the salinity of each solution determined from the ratio of conductivities measured by a Beckman induction salinometer (model RS 7B). These solutions were analyzed in the UltraPath system using Optima™ water as a reference blank, and are presented as optical density (negative base 10 logarithm of the light flux through the reference minus the light flux through the sample). The refractive index effect increased in magnitude with increasing salinity and was wavelength dependent (Fig. 2(A)). The overall curves were linear, and exhibited an approximate optical density of 0.003 (dimensionless) per salinity unit dependence. The root-mean-square deviation of the individual determinations from the least-squares regression line was 0.0019 (optical density) at 300 nm, 0.0018 at 325 nm, and 0.0014 at 400 nm. At oceanic salinities (33–37 on the practical salinity scale) the correction factor is close to −0.1 in the 300–550 nm wavelength range (Fig. 2(B)).

We determined the apparent optical absorbance spectra of filtered seawater samples at sea. Typically, samples were analyzed in batches of 12, with a blank determination before and after each batch. This allowed us to track instrument drift (lamp output or spectrometer sensitivity). The spectrometer collected data at 1 nm intervals with an effective slit width of 2 nm, and five spectra were collected from each sample over a 2-min period. The five spectra were averaged unless there was a time

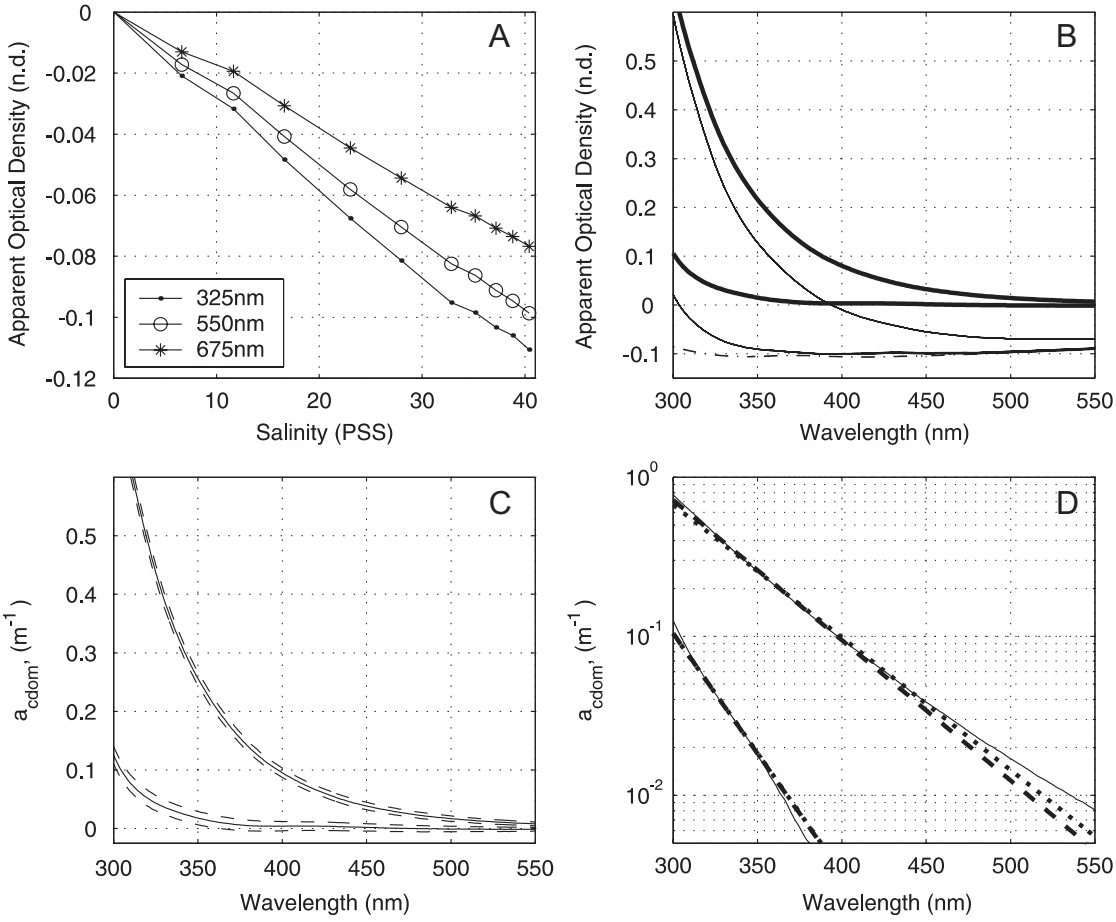

Fig. 2. Salinity dependent correction factors at selected wavelengths used for the UltraPath liquid waveguide spectrophotometer system in the present study. The correction factors were determined by using artificial seawater solutions of varying salinity. Correction factors were prepared from apparent optical density spectra (vs. Milli-Q water) measured at a 1 nm resolution. In the field, correction factors were interpolated for the exact salinity (based on salinometer analysis of bottle samples from which the CDOM samples were drawn, and were subtracted from the raw absorbance spectra to correct for the refractive index effect of seawater vs. fresh water blanks (see Methods).

trend in the spectra over the 2-min interval, in which case the spectrum was excluded from analysis. Standard deviation of the five scans was on average less than 0.0025 (dimensionless optical density), in the 325–412 nm spectral range, corresponding to $0.0028\,m^{-1}$ with the optical pathlength taken into account (see below). The raw spectra were corrected at each wavelength by interpolating the correction factor on the salinity of the sample (Fig. 2(A)) and subtracting the corresponding correction spectrum (Fig. 2(B)). The resulting dimensionless optical density spectra were converted to absorption coefficient (m^{-1}) by multiplying the spectrum by $2.303/l$, where 2.303 converts decadal logarithmic absorbance to base e, and l is the effective optical pathlength of the waveguide. For this waveguide the effective optical pathlength was 1.943 m and was determined at the factory through a linearity test using a Phenol Red dye standard buffered solution with an absorbance (optical density) of $1.0\,cm^{-1}$.

We assessed the overall precision of this method by means of replicate samples collected at 500 m at a station in the subtropical North Pacific in four separate Niskin bottles. From this set of spectra we computed a 95% confidence interval estimate spectrum which we apply as an uncertainty estimate in the present study (Fig. 2(C)). At 325 nm the uncertainty of a_{cdom} is approximately $0.013\,m^{-1}$, declining with wavelength to $0.007\,m^{-1}$ at 412 nm (Fig. 2(C)). Of this uncertainty less than $0.003\,m^{-1}$ (at 325 nm) can be attributed to electronic noise and repeatability (as assessed by replicate scans of the same sample within a minute, shown above). Uncertainty introduced by reinjection of the sample or blank is of a similar magnitude (not shown), as is suggested by deviations from linearity of the dilution series of ASW (Fig. 2(A)).

CDOM spectra, particularly in the visible waveband (400–700 nm) typically fit a wavelength dependent exponential function with a single slope parameter, S (nm^{-1}), such that $a_{cdom}(\lambda) = a_{cdom}(\lambda_o)e^{-S(\lambda-\lambda o)}$, where λ_o is a reference wavelength. We computed the slope parameter by fitting the spectrum from 320 to 650 nm to an exponential equation using a least-squares nonlinear curve fitting approach (Twardowski et al., 2004). We did not include shorter- or longer-wavelength portions of the spectrum because the shorter-wavelength portion of the spectrum does not fit a single exponential well (Nelson et al., 2004) and the longer-wavelength portion is strongly affected by temperature-dependent absorption by water (Pegau et al., 1997). We designate the parameter determined this way as S_{nlf}. We also estimated a hyperbolic slope parameter as described by Twardowski et al. (2004) but this parameter was highly linearly correlated to S_{nlf} ($R^2 > 0.9999$) so we here present only the more familiar S_{nlf} parameter. Nonlinear and linear fits to log-transformed a_{cdom} data are shown for example for CDOM spectra in Fig. 2(D). Both methods provide a good fit to the data where absorption coefficients are higher than ca. $0.03\,m^{-1}$, but deviate from the measured spectra at lower values.

2.4. DOC data

Concentrations of DOC (DOC, $\mu mol\,l^{-1}$) were determined from the same Niskin bottle from which CDOM samples were drawn. Samples were drawn into acid leached high-density polyethylene bottles and were frozen at −20 °C for later analysis at UCSB. Samples collected at depths 1000 m and shallower were subjected to inline gravity filtration through a combusted GF/F filter (polycarbonate filter holders were attached directly to the Niskin spigots so no additional water handling or apparatus were required). DOC analyses were performed at shore laboratories within 3–9 months of sample collection. All samples were analyzed via the high temperature combustion technique using a modified Shimadzu TOC-V analyzer. DOC analyses followed established methods detailed in Carlson et al. (2004).

2.5. CFC-derived ventilation ages

To analyze the spatial distribution of CDOM within the deep ocean water masses, we calculate estimates of water ventilation age using measurements of CFC concentration (e.g., Doney and Bullister, 1992). We used CFC-12 measurements for this purpose because its concentration in the atmosphere continued to increase until 2001, compared to CFC-11 and CFC-113 concentrations, which ceased to increase in 1993, and thus it has a longer range for pCFC ages. Values of the partial pressure of CFC-12, pCFC-12, were computed as the quotient of the CFC-12 concentrations measured in bottle samples and the solubility constant, which is a function of temperature, salinity and pressure (Warner and Weiss, 1985). The time series of the Northern Hemisphere CFC-12 atmospheric mole fraction (Walker et al., 2000) was extended

through 2003 using atmospheric measurements made at Trinidad Head, California as part of the AGAGE project (Prinn et al., 2000) and reported on the CDIAC website ⟨http://cdiac.ornl.gov/ftp/ale_gage_Agage/AGAGE/⟩. The ventilation year was estimated by comparing the pCFC-12 values to the annual averages of CFC-12 in the atmosphere as a function of time and the pCFC-12 age was found by subtracting the ventilation year from the year of collection. We disregarded all values where CFC-12 concentration was less than or equal to 0.02 pmol kg^{-1} which corresponds to a pCFC-12 value of about 5 μatm in our data set and a ventilation age estimate of about 55 years. At this concentration the relative error on the measurement is large and there is likely to be a significant admixture of CFC-free water in the water mass; both of these factors cause large errors in the pCFC age, as will be discussed below. The mole fraction of CFC-12 in the atmosphere reached a maximum annual average of 547.2 μatm in 2001 and 2002, then decreased to 546.8 μatm in 2003; thus it is not possible to distinguish between ages of 0–3 years. The precision of the CFC-12 method is often approximately the larger of 0.5% or 0.01 pmol kg^{-1} for a single laboratory, which was the case for the A20 and A22 cruises, but comparisons between the numerous WOCE data sets measured by different laboratories reveal a practical precision and accuracy of 1–3% (Fine et al., 2002). The error in the pCFC-12 age resulting from the analytical uncertainty varies as a function of the slope of the CFC-12 vs. time for the atmospheric concentration curve. The minimum estimated error in ventilation age is approximately 0.5 years for pCFC-12 ages between 5 and 45 years. For ages between 45 and 55 years the error increases from about 0.5 to 2 years and for ages between 3 and 5 years, the error is about 1 year.

CFC-12 measurement accuracy is not the only source of error in estimating ventilation age from pCFC-12 measurements. Undersaturation of CFC-12 in surface waters at the time of ventilation (Doney and Jenkins, 1988, Haine and Richards, 1995, Fine et al., 2002), which results from rapid deep mixing during winter, and mixing of 'newer,' high-CFC water with 'older' low CFC water (Doney et al., 1997, Smethie et al., 2000) also perturb age estimates from CFC concentration. To account for the undersaturation factor, pCFC-12 ages were estimated using our best estimate of the CFC-12 saturation level in the source water region for each layer (Table 1). In cases of undersaturation, the atmospheric time history was multiplied by the fraction of saturation and then the year of formation determined from the pCFC value of the water samples. In some cases for surface and near SURF, the pCFC value was greater than the saturation-adjusted maximum in the atmospheric time history. This results when water becomes supersaturated, which occurs from water warming by increased solar radiation in spring and summer and by mixing with warmer water. For these cases, the age was assumed to be zero. Mixing of water masses bearing differing CFC concentrations interacts with the atmospheric CFC time history to bias age estimates (Doney et al., 1997). Restricting our pCFC age calculation to CFC-12 concentrations above 0.02 pmol kg^{-1} eliminates situations where the problem of mixing zero-CFC "old" water with more recently ventilated CFC-bearing water is most acute, but waters in the older part of the age range that we use probably have a mean age that is greater than the pCFC-12 age. The effect of this can be estimated by a more extensive analysis of the CFC and other tracer data to generate an age spectrum (Waugh et al., 2004), but this is beyond the scope of this paper.

3. Results and discussion

The observations presented here represent the first systematic survey of the colored DOM distribution of the North Atlantic Ocean including sampling of all water masses from the surface ocean through the deep sea. As such, these data along with the hydrographic observations available from the Repeat Hydrography surveys provide clues of the processes controlling the oceanic CDOM distribution and its implications. In the following, we first discuss the results of the transient tracer age distribution analysis on the described sections, as these data are used in the subsequent sections. We then address the processes controlling the CDOM distribution in SURF, the subtropical mode water (STMW), and deep ocean water masses including the main thermocline, AAIW, and NADW layers. Next we focus on features of CDOM diagenesis that can be described from these results. Last, we end with a discussion of the utility of CDOM as semi-conserved tracer of biogeochemical process.

3.1. Estimated ventilation ages

Distribution of pCFC-12 age in the western North Atlantic (Fig. 3) reflects features of the

general circulation (Smethie et al., 2000; Smethie and Fine, 2001). The major features of interest to us in the present research are the gradients in pCFC-12 age vs. latitude within the principal subsurface water masses. In STMV, ages range from the 0–3 years to about 15 years with older ages generally in the densest part of the water mass. For LTCL, youngest ages of 5–15 years are found just south of the Gulf Stream on both the 66°W and 52°W sections and increase in the southward direction to 15–30 years with higher ages in the most dense part of the water mass. The same pattern is observed for AAIW, but the age range is from about 25–30 years at the northern end of the sections to 50–55 years at the southern ends of the section and there is an extensive region with ages greater than 50 years south of 22°N along the 52°W section. For LSW, ISOW and DSOW, the age pattern is similar with youngest ages at the northern end of the sections in the DWBC, oldest ages in the center of the sections in the interior and intermediate ages at the southern ends in the DWBC. Following the flow path of the DWBC (north end of A20, north end of A22, south end of A22 (excluding Caribbean Sea), south end of A20), the pCFC-12 ages increase from 20–25 years to 26–28 years to 34–35 years to 37–38 years for LSW; 28–32 years to 32–36 years to 42–43 years to 47–48 years for ISOW; and 31–32 years to 33–34 years to 40–41 years to 43 years for DSOW. The ages in the interior increase to 49 years for LSW and to greater than 55 years for ISOW and DSOW. AABW is observed in the interior and at the southern ends of both sections with ages no greater than about 52 years. In the Caribbean Sea, which contains deep water with a density similar to that of LSW, the deep ages are about 55 years.

Water mass ages are generally considered to be the time required for the water to travel from its region of formation near the surface to the point where it was sampled. The mean age is the average of the ages of all of the components of a water parcel and is the age that is most appropriate for calculating degradation rates of organic matter or any substance from its measured field. The pCFC-12 age gives an approximation of the mean age if none of the water parcel components formed prior to the time of CFC-12 input to the oceans. This is the case for most of the thermocline waters and STMW in the North Atlantic, but denser water masses do contain components that formed prior to CFC-12 input. This is particularly true for AABW and AAIW in the North Atlantic and indeed the CFC-12 signal in these water masses in the North Atlantic are from mixing with other water masses of North Atlantic origin that contain CFCs. We used the best estimates of the CFC-12 saturation in the formation regions for all of the water masses. This is not the correct procedure for AABW and AAIW since the CFC-12 signal from the regions of formation of these water masses in the Southern Ocean has not yet reached the North Atlantic Ocean. However, the saturations are not much different than the saturations for the North Atlantic source waters (Table 1) and this assumption introduces little more uncertainty than already exists from the effect of mixing

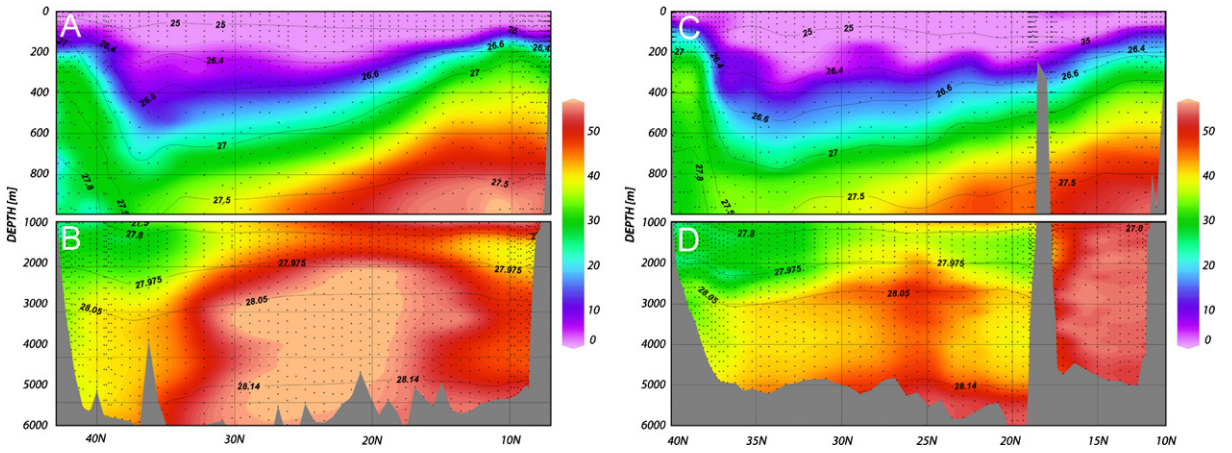

Fig. 3. Distribution of pCFC-12 derived age estimate (year) along 52°W (A20 section, (A) and (B) and 66°W A22 section, (C) and (D)) overlaid with the contours of neutral density corresponding to the water mass definitions shown in Table 1. Note that the contours are not regular intervals. Panels (A) and (C) cover the depth range 0–1000 m, and panels (B) and (D) cover the depth range 1000–6000 m for the A20 and A22 sections, respectively.

between CFC-bearing and CFC-free waters that was discussed earlier. However, this procedure does produce age gradients with the correct sign and allows limits to be placed on the production or degradation rates of CDOM reported in this paper.

The ages for LSW and DSOW in the DWBC reported here are older than previous estimates from transient tracer data. The age of LSW has been estimated to increase from about 10 years just south of the Grand Banks to 25–30 years at the equator (e.g. Weiss et al., 1985; Smethie et al., 2000) compared to a range of 20–25 years just south of the Grand Banks to 37–38 years at 8°N for data used in this study. For DSOW, the age has been estimated to be 10–15 years just south of the Grand Banks and about 25 years at the equator (e.g. Doney and Jenkins, 1994; Smethie et al., 2000), compared to 31–32 years to 43 years from this study. Tracer ratios (CFC-11:CFC-12 and He-3:tritium) were used to estimate the ages in these earlier studies, and ratios and thus ages estimated from them are not affected by mixing with zero or very low tracer water. Ages calculated by this technique yield an estimate of the youngest component of a water parcel and hence are lesser than the mean age. However, the age gradient in the DWBC is roughly the same for both techniques, 15 years between the Grand Banks and the tropics.

3.2. Control of CDOM in surface waters

The meridional distribution of CDOM (defined here as dissolved absorption coefficient at 325 nm, m^{-1}) in samples taken at the surface (depths $\leqslant$ 10 m) along the three sections is shown in Fig. 4. The highest values were found on the continental shelves (N. and S. American), in the slope waters inshore of the Gulf Stream, in the western tropical Atlantic (possibly under the influence of the Amazon plume, Del Vecchio and Subramaniam, 2004), and in the Caribbean (presumably influenced by the Orinoco plume, Blough et al., 1993; Siegel et al., 2002). These high CDOM values presumably represent terrestrial influence, from coastal runoff and rivers (Siegel et al., 2002). The lowest values were found in the Sargasso Sea (North Atlantic subtropical gyre), where stratification and high solar radiation levels leading to bleaching counters local production of CDOM (Nelson et al., 1998). Intermediate CDOM values were found in the North Atlantic subpolar

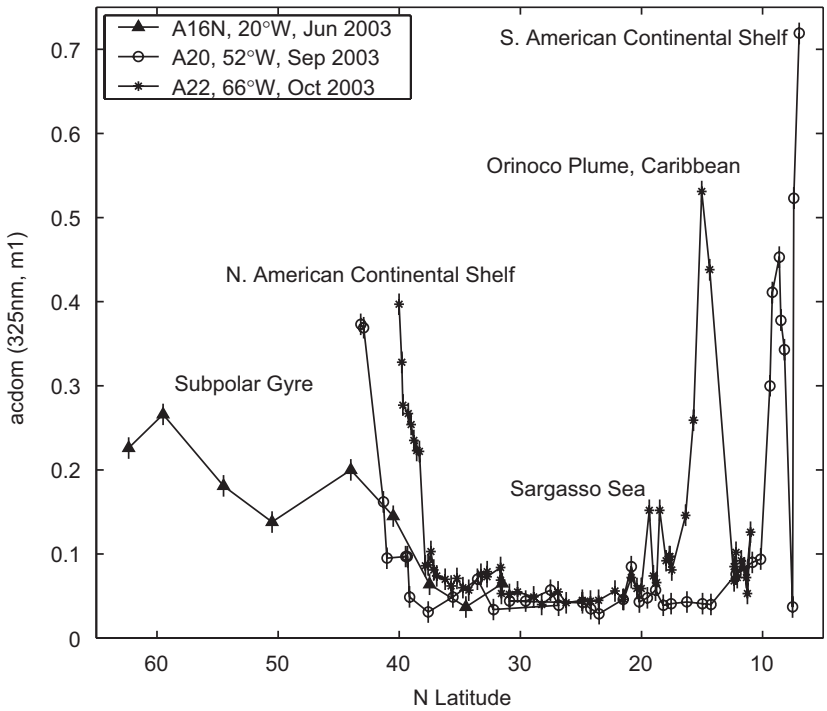

Fig. 4. Distribution of CDOM (as absorption coefficient at 325 nm, m^{-1}) in surface water samples (depths 0–5 m) collected in the present study, plotted against latitude. Symbols denote samples from the different sections as shown in Fig. 1. Error bars are the 95% confidence interval for a single estimate (see Methods).

gyre waters, where absorption coefficients of CDOM at the surface were approximately four-fold higher than in the Sargasso Sea despite the absence of obvious terrestrial influence. This difference presumably reflects reduced bleaching because of lower insolation, greater mixing, and higher biological productivity. Where the sections overlapped latitudes in the subtropical gyre (between 30°N and 40°N for all three transects, between 20°N and 40°N for A20 and A22), surface CDOM abundances were similar (Fig. 4). The basin-scale pattern of CDOM abundance shown in our in situ measurements corresponds well to satellite views of the CDOM distribution (Siegel et al., 2002, 2005a, b).

Surface (top 200 m) vertical profiles of CDOM absorption coefficient can be sorted into several distinct patterns. In subpolar waters (62°N), values of CDOM are at their maximum near the surface (Fig. 5(A)), declining to approximately half that value in the top 100 m. In subtropical waters, the case is reversed: a steep increase in CDOM absorption coefficient (up to 4 ×) is observed between the mixed layer and approximately 100 m, coincident with the seasonal thermocline (Fig. 5(C)). These profiles had relatively low resolution in surface waters (ca. 25 m bottle spacing) so the position of the subsurface maximum is approximate. Data from BATS (Nelson et al., 1998) indicate that the peak in the subsurface CDOM profile in subtropical waters is actually shallower than 100 m. Below 100 m, values of CDOM decline. Within continental slope and shelf waters the pattern is similar to the open ocean subpolar profiles, with a larger surface concentration (Figs. 5(B) and (D)). Some stations on the continental shelf and slope exhibited evidence of current or previous stratification and bleaching (Fig. 5(B)). CDOM profiles in the surface waters are seen to be determined by the interactions between bleaching and input (either allochthonous or autochthonous), as seen by Nelson et al. (1998). It is apparent from the subpolar and continental slope vertical profiles that production or input processes likely occurs near the surface, and CDOM concentration is lower in the main thermocline and the deep ocean (with the exception of the subtropical gyres). This pattern supports the notion that solar bleaching is the largest sink of CDOM in surface waters, and that open ocean CDOM distributions require both terrestrial and open ocean sources, with open ocean sources dominating (Siegel et al., 2002).

Contours of CDOM in the top 1000 m of the A20 and A22 sections are shown in color in Figs. 6(A) and (C). The corresponding 1000–6000 m sections are shown in Figs. 6(B) and (D). The A16N section is not shown in contour form because of the sparseness of the data set. At the surface, the surface lens of low CDOM in the subtropical gyre is easily seen, as are the high CDOM values found on the continental shelves. In the Caribbean portion of the A22 section (Fig. 6(C)), surface to 100 m CDOM values are higher than in the central gyre despite the fact that both have well-stratified water columns. The feature we consider to be a relict of the Orinoco plume is visible near 15°N at depths shallower than 100 m (Figs. 5(D) and 6(D)). The subsurface maximum in subtropical waters at ca. 100 m is seen spanning the central gyre in both sections. Below this lies a broad minimum in the CDOM profile coincident with the STMW.

4. CDOM in the STMW, thermocline, and intermediate waters

The STMW lies between the seasonal or surface thermocline and the main thermocline within the subtropical gyres, and is often defined hydrographically as encompassing a local minimum in the profile of PV (Worthington, 1959; Talley and Raymer, 1982). Circulation of STMW in the North Atlantic is presumed to follow the Gulf Stream recirculation from northeast to southwest (Worthington 1976, Joyce et al., 2000; Alfutis and Cornillon, 2001). In the Sargasso Sea, STMW is ventilated during the winter on an occasional (mostly annual) basis in a region north of Bermuda and south of the Gulf Stream (e.g., Talley and Raymer, 1982). Joyce et al. (2000) have adopted the 26.4 and 26.6 $kg\,m^{-3}$ isopycnals of neutral density (γ^n) as the vertical boundaries of the core of the STMW in the Sargasso Sea. Fig. 6 shows the neutral density boundaries of the STMW (and the AAIW) overlain as contours on a field of the absorption coefficient of CDOM at 325 nm (m^{-1}). It can be clearly seen that the STMW represents an intermediate minimum in the CDOM profile and defines the near-100 m subsurface maxima observed in the profiles (Fig. 5(B)). The STMW signature is most pronounced in the northern latitudes of A20 (Fig. 6(A)) and A22 (Fig. 6(C)) sections. In both the A20 (Fig. 6(A)) and A22 (Fig. 6(C)) sections the STMW is thickest in the region of 35°N (near where mode water is ventilated) and thins to the south. Below the mode water the concentration of CDOM

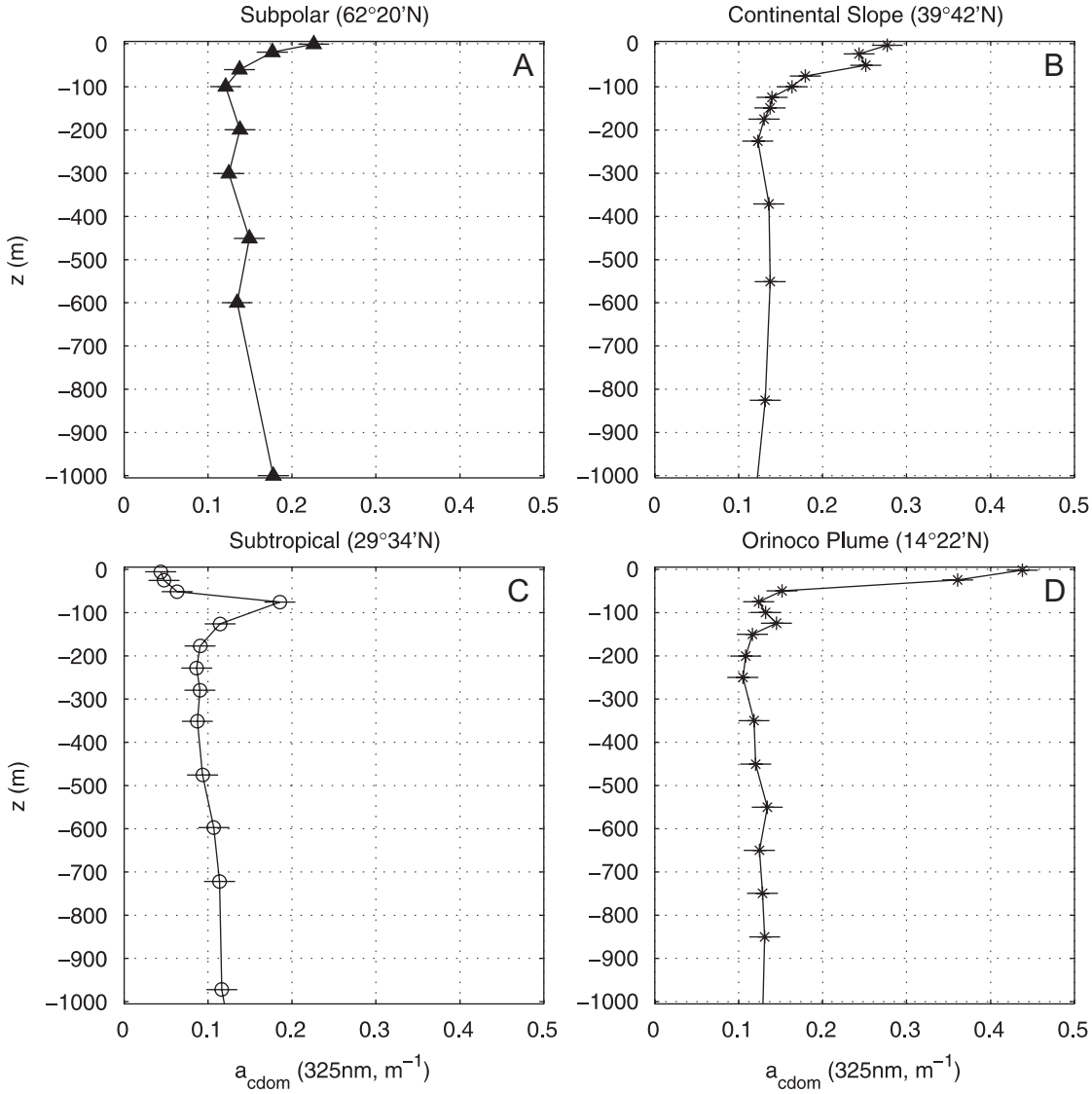

Fig. 5. Selected profiles of CDOM (absorption coefficient at 325 nm, m^{-1}) in the top 1000 m collected from different oceanographic provinces in the North Atlantic in the summer of 2003. The impact of solar bleaching in stratified subtropical conditions can be seen in (C), contrasted with the unbleached surface waters in the subpolar gyre (A) and on the continental shelf (B) and the very high surface lens of CDOM from the Orinoco plume (D). Symbols denote the different sections as shown in Fig. 1.

in the main thermocline is roughly equal to that of the subsurface maximum.

Within the STMW the concentration of CDOM is variable, ranging from an absorption coefficient of less than 0.075 m^{-1} at 325 nm to over 0.1 m^{-1}. In general CDOM abundance is greater to the south where the mode water thins, but in both the A20 and A22 sections there are low CDOM features which span $>$ 200 km interspersed with higher CDOM features (Figs. 6(A), (C) and 7). This pattern was more pronounced along the A20 section at 52°W (Fig. 7(A)) than it was along the A22 section at 66°W (Fig. 7(B)). Of note is that no significant correlation exists between the CDOM sampled in the STMW along these two sections and the corresponding salinity and PV (data not shown). Along the A20 section at 35°N just south of the Gulf Stream (Fig. 5(A)) there is a local maximum in CDOM found between 80 and 800 m (spanning the seasonal thermocline, the STMW and the main thermocline), which is also reflected in the neutral density contours. A local low in sea surface height

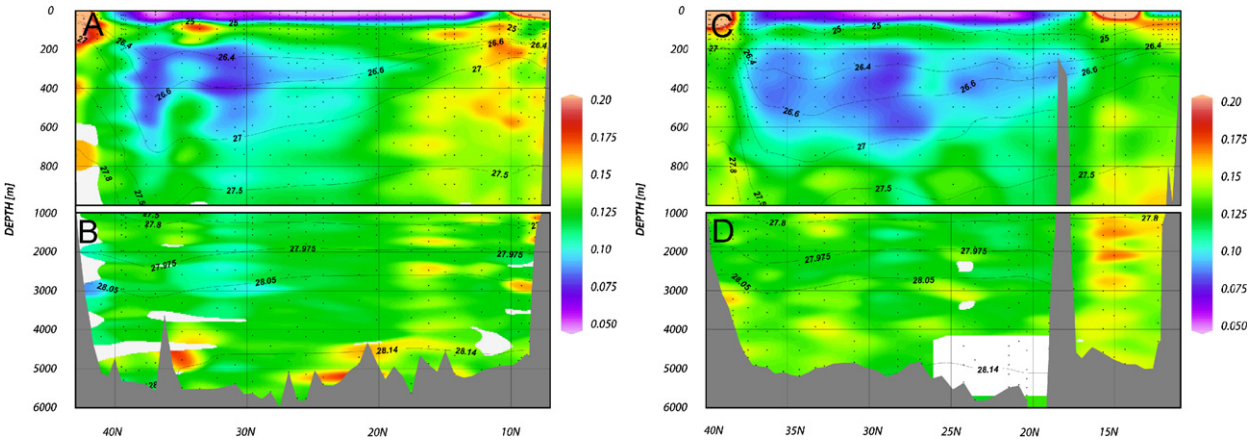

Fig. 6. Distribution of CDOM (as 325 nm absorption coefficient, m^{-1}) along 52°W (A20 section, (A) and (B)) and 66°W (A22 section, (C) and (D)), as in Fig. 3.

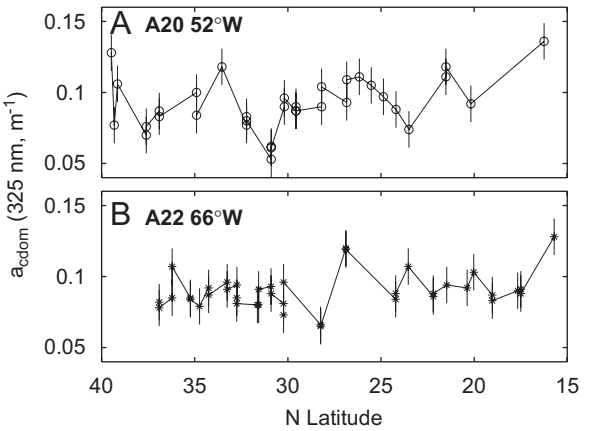

Fig. 7. Distribution of CDOM (as 325 nm absorption coefficient, m^{-1}) within the subtropical mode water (defined as neutral density interval between 26.4 and 26.6 kg m^{-3}) along the A20 line, 52°W (A) and the A22 line, 66°W (B). Error bars are the 95% confidence interval for a single estimate (see Methods).

anomaly is also visible in satellite altimetry analyses from this area (not shown). We provisionally identify this feature based on the isopycnal deflections as a cyclonic eddy or cold core Gulf Stream ring, and the higher CDOM in this location may be a consequence of advection or local higher productivity (McNeil et al., 1999, McGillicuddy et al., 1999).

Within the STMW, a statistically significant relationship between CDOM and pCFC-12 age (Fig. 8(A)), and CDOM and AOU (Table 2) is evident, but no statistically significant relationship between CDOM and PV was found (not shown). This suggests that the state of the mode water at the time of formation, and in situ production of CDOM through remineralization processes (which would increase CDOM with age and correlate with AOU), both contribute to the observed spatial variation in STMW CDOM.

These processes appear to be more important than diapycnal mixing (which would increase PV and CDOM in parallel, e.g., Palter et al., 2005), in determining the CDOM concentration within the STMW along the transects. From the low value of R^2 in the CDOM–ventilation age correlation, it is apparent that new formation of CDOM is a minor contributor to CDOM variability in the mode water, so conditions at the time of formation are the most important.

Environmental conditions that govern the formation of mode water include the extent and severity of cold-air outbreaks during winter and wind in the formation area, which controls the maximum depth of the winter surface, mixed layer (Joyce et al., 2000; Alfutis and Cornillon, 2001). These factors would determine the CDOM concentration at the time of mode water formation as well as the history of the mixed layer and irradiance over the time scales appropriate for significant photobleaching of CDOM (Nelson et al., 1998).

It would appear from our present results that the processes which result in lower PV water parcels during periods of formation are not correlated with high or low CDOM abundance at the time of STMW ventilation. Further, no significant temporal relationship between indexes of the North Atlantic Oscillation, ENSO, and CDOM within the STMW was found using pCFC-12 age (results not shown).

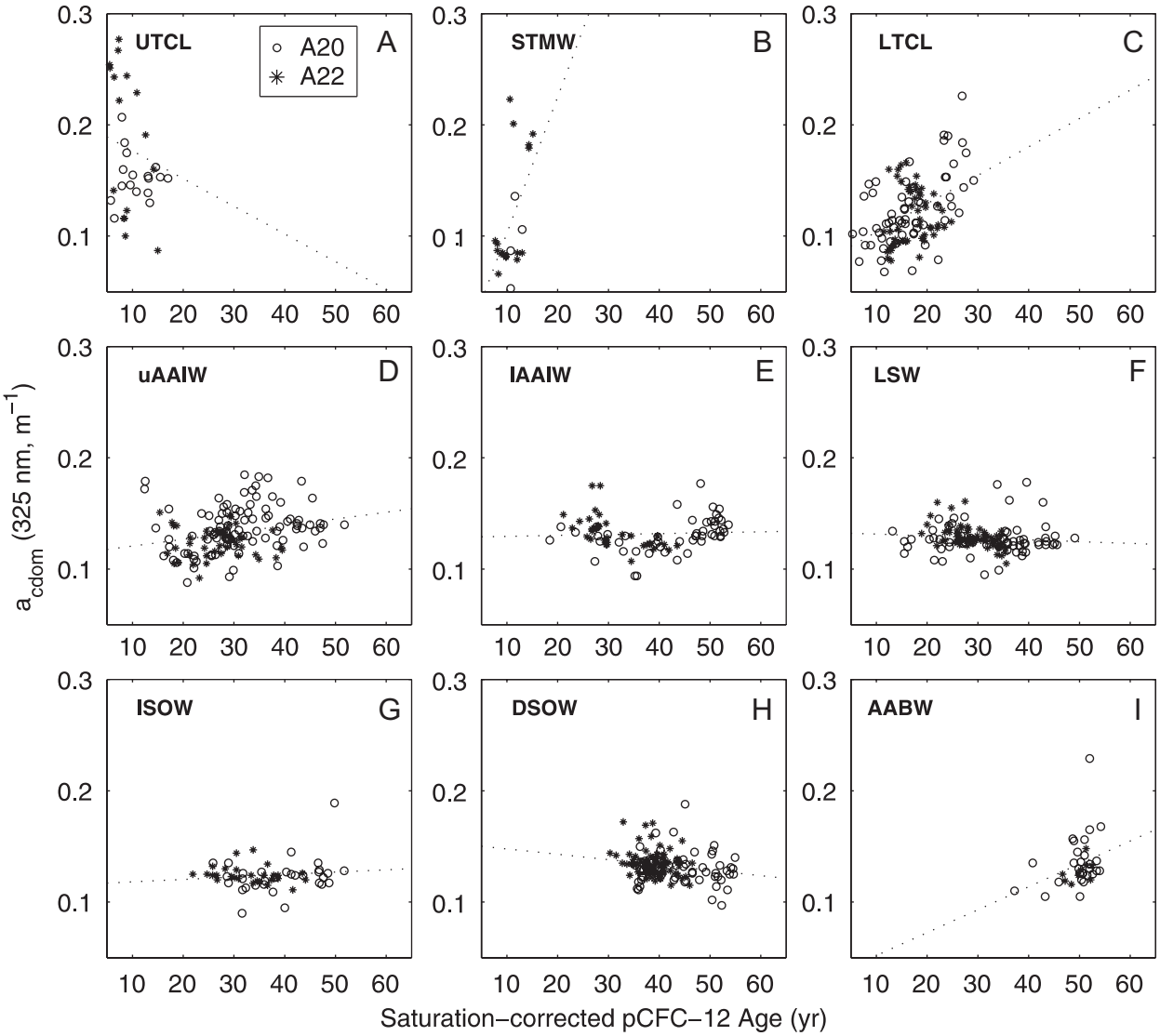

Fig. 8. Scatter plots of CDOM (absorption coefficient at 325 nm, m^{-1}) vs. pCFC-12 age (year) for water masses discussed in the present study (Table 1), with the surface layer omitted. (A) Upper (seasonal) thermocline (UTCL). (B) Subtropical mode water (STMW). (C) Lower (main) thermocline (LTCL). (D) Upper Antarctic intermediate water (uAAIW). (E) Lower Antarctic intermediate water (lAAIW). (F) Labrador Sea water (LSW). (G) Iceland–Scotland overflow water (ISOW). (H) Denmark Strait overflow water (DSOW). (I) Antarctic bottom water (AABW). Symbols indicate samples taken from the A20 (○) and A22 (*) lines. Overlaid lines are least-squares linear regression lines (Table 2).

These results emphasize the decoupling between the convective processes that renew the mode water and the biological plus physical processes (synthesis and bleaching) that control the CDOM profile between renewal events.

Weak yet statistically significant increases of CDOM were correlated with increases in apparent ventilation age in the main thermocline and the upper AAIW (Fig. 8 and Table 2). The apparent increase rate of CDOM decreased with depth (Table 2), and CDOM increase in these layers was also weakly but significantly correlated with increases in AOU. AOU is often used as a proxy for past microbial remineralization; this result therefore suggests that remineralization of organic matter resulted in net production of CDOM below the euphotic zone, and that CDOM production decreased with depth (Table 2) (Coble et al., 1998;

Table 2
Regression statistics for CDOM abundance (absorption coefficient at 325 nm) vs. pCFC-12 age (Fig. 8) CDOM abundance vs. AOU, and CDOM spectral slope parameter (S_{nlf}, nm^{-1}) vs. pCFC-12 age by layer, as defined in Table 1

Layer	CDOM vs. age ($m^{-1}yr^{-1}$)	R^2	n	t-test	CDOM vs. AOU ($m^{-1}(\mu mol\,kg^{-1})^{-1}$	R^2	N	t-test	S_{nlf} vs. age ($nm^{-1}yr^{-1}$)	R^2	n	t-test
SURF	0.005	0.031	80	N.S.	0.0009	0.034	52	N.S.	−0.0003	0.020	80	N.S.
UTCL	−0.002	0.019	48	N.S.	0.0002	0.004	209	N.S.	−0.0003	0.194	48	$P<0.025$
STMW	0.0100	0.028	20	$P<0.025$	0.002	0.464	76	$P<0.025$	−0.0006	0.181	20	$P<0.025$
LTCL	0.0030	0.197	113	$P<0.025$	0.0003	0.087	125	$P<0.025$	−0.0002	0.100	113	$P<0.025$
uAAIW	0.0006	0.064	144	$P<0.025$	0.0002	0.075	157	$P<0.025$	−0.0001	0.164	144	$P<0.025$
lAAIW	8 E-5	0.003	83	N.S.	2 E-5	0.002	87	N.S.	−0.0001	0.246	83	$P<0.025$
LSW	−0.0002	0.010	131	N.S.	-6 E-5	0.004	135	N.S.	−4 E-5	0.014	131	N.S.
ISOW	0.0002	0.016	58	N.S.	9 E-5	0.002	63	N.S.	−0.0001	0.134	58	$P<0.025$
DSOW	−0.0005	0.042	138	$P<0.025$	7 E-5	0.002	152	N.S.	−9 E-5	0.056	138	$P<0.025$
AABW	0.002	0.107	37	$P<0.025$	0.0001	0.007	43	N.S.	−2 E-5	0.000	37	N.S.

Caribbean and Eastern Atlantic (A16N) data are omitted from this analysis. R^2 = squared linear correlation coefficient. n = number of samples. N.S. = not significant at a 95% level of confidence ($P >= 0.025$, 2-tailed t-test).

Nelson and Siegel 2002; Nelson et al., 2004). The pCFC-derived age estimates we are using work best in the main thermocline (Smethie et al., 2000) so we have confidence in this assertion, but it is difficult to be quantitative. It is apparent from the R^2 values that remineralization is at best a minor contributor to the variability in CDOM in these layers, accounting for less than 20% of the variability.

Water masses in the AAIW are expected to be low in CFC-12 concentration (and thus have large apparent ages) because of the great distance from the North Atlantic to their source waters, but in our data set this is not the case. Mixing with higher CFC-12 waters in the well-ventilated North Atlantic decreases the apparent ventilation age to the range observed and the older AAIW component of the mixture may introduce higher CDOM waters.

4.1. CDOM in the deep ocean water masses

Deep ocean water masses sampled along the transects in the present study include the NADW and AABW (Joyce et al., 1999; Hall et al., 2004). Generally, CDOM (as 325 nm optical absorption coefficient) increased with depth in the main thermocline and remained at a value of 0.125 to 0.2 m^{-1} throughout the deep North Atlantic (Figs. 6(B) and (D)). Deep water masses have slightly higher concentrations of CDOM to the south, which presumably reflects the recirculation of NADW (Smethie et al., 2000), in which CDOM may be higher because of a remineralization source. CDOM is also relatively high (ca. 0.15 m^{-1}) in the deep (>1000 m) waters of the Caribbean (Fig. 6(D)) which may also be because of remineralization occurring over longer time in the much less-recently ventilated water.

Below the subtropical gyre or between 15°N and 35°N, mean values of CDOM in the AAIW, NADW and AABW layers were similar on the two sections. The deep ocean mean CDOM values were also higher than the STMW and surface values. Average concentrations of CDOM in the AAIW fell between those of the STMW and the NADW between 25°N and 30°N along 66°W (Fig. 6). In all cases the standard deviations were large and overlapped values on the shallower and deeper layers.

The CDOM distribution in the deep ocean water masses was relatively homogenous compared to that of surface and intermediate waters (Fig. 6), and had weak or absent trends with pCFC-12 age (Table 2). We interpret these results as reflecting rapid turnover

of the water masses because of advection and isopycnal mixing (Smethie et al., 2000, Waugh et al., 2004). If advection were slower, accumulation of CDOM from remineralization would occur in the deep ocean layers, but this is only observed in the STMW, thermocline, and upper AAIW. Even this accumulation is extremely slow, with turnover times relatively long compared to presumed ventilation turnover times. Diapycnal mixing would homogenize CFC-12 ventilation age signals along with the CDOM, so this is also unlikely to completely explain these patterns. Instead we believe the CDOM signals at depth in the North Atlantic Deep Water primarily reflect the CDOM abundance at the location and time of formation, similar to what is observed in the STMW but over longer distances and times.

In the DSOW, the weak but significant decline in CDOM abundance vs. age (Fig. 8(H) and Table 2) is mostly driven by a difference between the A20 transect (○) and the A22 transect (*). DSOW lies between layers that have lower and higher CDOM (ISOW and AABW), so it is possible this trend is driven by differential mixing at different locations, as are the artificially low ages of the AAIW layers. This effect is likely to be larger along the A20 transect because of the larger meridional and vertical gradients of CFC-12 (e.g. Fig. 8). No correlation with AOU was found in this layer (Table 2), suggesting that the decrease in CDOM was not due to microbial consumption, which has been documented to occur in culture experiments (Nelson et al., 2004).

There was also a significant positive correlation between CDOM and pCFC-12 age in the AABW layer, but this relationship explains only ca. 10% of the variance in CDOM. We suspect this relationship to be spurious, as most of the points are clustered near the maximum age estimated using the techniques used in the present study. We believe the significant increasing trend of CDOM within the AABW to be an artifact of the ventilation age estimation technique, as most of the points are near the upper limit of estimation. However, if this trend is real, a possible source of CDOM to the AABW may be bottom sediments, which are significant sources of CDOM to neritic waters (Chen and Bada, 1994; Boss and Zaneveld, 1993).

4.2. CDOM spectral properties

The spectral slope of the CDOM absorption spectrum is presumed to reflect to a certain degree the chemical composition and state of the chromophores in the pool (Del Vecchio and Blough, 2004). In the present study we examine the spatial variability of the slope parameter in the context of hydrography and water mass age, to test whether this parameter is a useful tracer of origin or diagenetic state of CDOM. In general, absorption coefficient of CDOM and the spectral slope parameter vary inversely (Twardowski et al., 2004). High values of the CDOM spectral slope parameter ($> 0.02\,nm^{-1}$) are often used to diagnose the past history of photobleaching (Green and Blough, 1994), but can also be an indicator of newly produced CDOM (Nelson et al., 2004). Low values of S_{nlf} ($< 0.016\,nm^{-1}$) have been linked with terrestrial-origin CDOM (Green and Blough, 1994, Del Vecchio and Subramaniam, 2004). But the overall distribution of CDOM spectral slope parameter has not been assessed across ocean basins and in the ocean interior.

The mean abundance of CDOM (as 325 nm absorption coefficient) within each layer (cf. Table 1) is shown in Fig. 9(A) (error bars are standard deviation). As in Fig. 8, the data shown here are from the A20 and A22 lines exclusive of the Caribbean. The lowest mean and highest variance is found in the SURF, which encompass the continental shelves and the permanently stratified subtropics. Highest values are found in the UTCL, with similar values in the deep ocean below the main thermocline. A similar plot showing mean values of the spectral slope parameter (S_{nlf}, nm^{-1}) is shown in Fig. 9(B). As is often the case, spectral slopes vary roughly inversely with absorption coefficient, but there are noticeable differences. The upper (seasonal) thermocline (UTCL) has a slightly higher mean slope value *and* higher CDOM abundance than the main (lower) thermocline (LTCL), while the STMW has mean abundance and slope parameter values falling between UTCL and surface layer values. The lowest mean S_{nlf} values were found in the AAIW and AABW layers. Low values of S_{nlf} (ca. $0.015\,nm^{-1}$) were also found in the subSURF of the Caribbean (not shown).

Scatter plots of S_{nlf} vs. estimated pCFC-12 age are shown in Fig. 10, which is similar to Fig. 8. In all layers, S_{nlf} decreased with increasing ventilation age. And, in all layers except for the surface (Fig. 10(A)), LSW (Fig. 10(F)), and AABW (Fig. 10(I)), there were statistically significant relationships between S_{nlf} and age (Table 2). As in the relationships between CDOM and ventilation

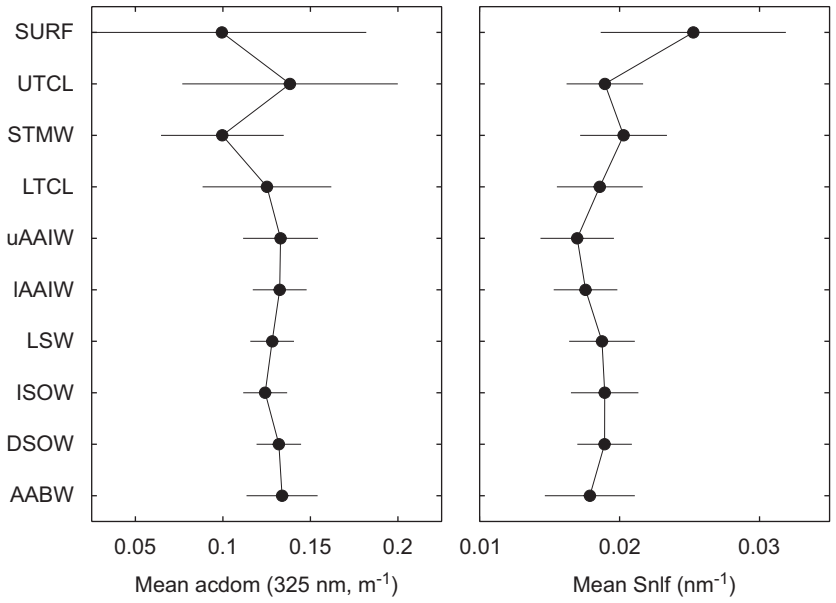

Fig. 9. Mean CDOM absorption coefficients (325 nm, m^{-1}) for samples collected within each layer (cf. Table 1). Error bars are the standard deviation.

age, these relationships were small in magnitude, indicating a long turnover time, and explained a small amount of the total variability in S_{nlf}.

4.3. DOC-specific absorption coefficient of CDOM

CDOM chromophores are part of the DOC pool, though are thought to be a rather small fraction (Nelson and Siegel, 2002). In the open ocean, the relationship between CDOM and DOC is not constant and the surface layer CDOM vs. DOC relationship will vary with the amount and quality of the terrestrial DOM input and the integrated effects of solar bleaching for a water parcel (e.g., Vodacek et al., 1997; Del Castillo et al., 1999; Nelson and Siegel 2002; Siegel et al., 2002; Del Vecchio and Blough, 2004; Conmy et al., 2004). In the ocean interior, changes in this relationship may reflect, for example, differential consumption (or production) of CDOM and DOC by microbes. We can examine the changes in DOC quality induced by these processes by examining the specific absorption coefficient of CDOM, or the quotient of CDOM absorption coefficient and DOC concentration, which we will denote a^*_{cdom}. Values of DOC-specific absorption coefficient of CDOM (a^*_{cdom}, units of $m^2\,g^{-1}$) are calculated by dividing the measured CDOM absorption coefficient at 325 nm (m^{-1}) by the DOC concentration ($g\,m^{-3}$) measured from the same bottle. Increases in a^*_{cdom} would then reflect either an increase in CDOM relative to the total DOC, or decreases in DOC without a corresponding change in CDOM.

The lowest values of a^*_{cdom} were found in SURF in the subtropical gyre where a^*_{cdom} values are 3–4 times lower than values found within the UTCL (Figs. 11(A) and (C)). The highest a^*_{cdom} values near the surface were found on the South American (Fig. 11(A)) and North American continental shelves (Fig. 11(C)), but not on the Grand Banks (Fig. 11(A)). There values of a^*_{cdom} near $0.3\,m^2\,g^{-1}$ were found at depths of ~100 m, below the depths where bleaching of CDOM in the mixed layer would occur. This is similar to the surface values of a^*_{cdom} in the subarctic gyre along the A16N transect (not shown), where terrestrial influence is low. This suggests that terrestrial-origin CDOM may have a higher a^*_{cdom} than that produced in situ, but the station where the Orinoco plume was observed at the surface (Fig. 11(C)) had a lower a^*_{cdom} value than nearby continental shelf stations. This may reflect partial bleaching of the CDOM within the plume, assuming the transport time from the estuary was significant (e.g., Del Castillo et al., 1999).

Below the surface, a^*_{cdom} is relatively high (~$0.23\,m^2\,g^{-1}$) in the upper (seasonal) thermocline (UTCL), but dips down in the STMW and main thermocline (Fig. 12(A)). Within the intermediate

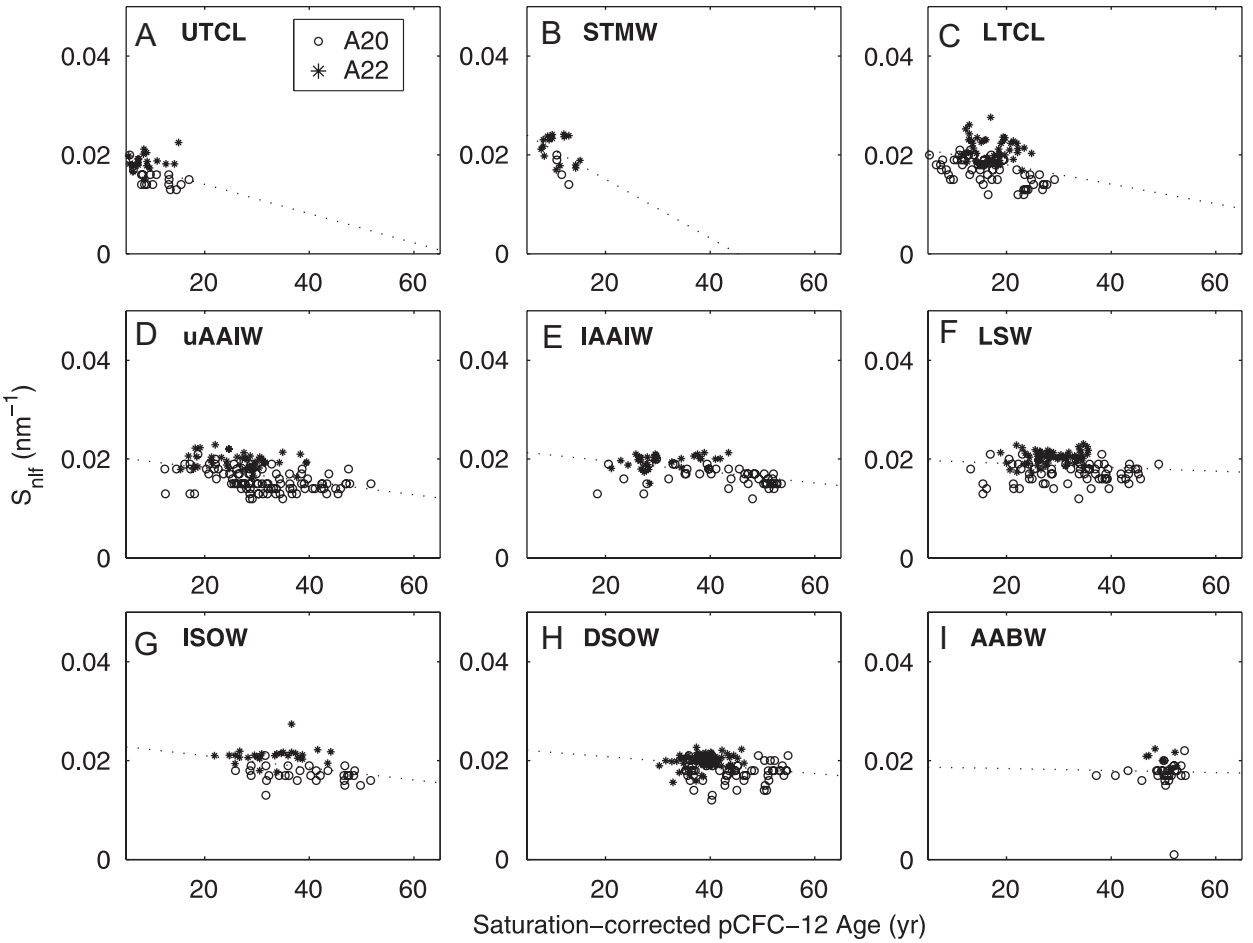

Fig. 10. Scatter plots of CDOM spectral slope parameter (S_{nlf}, nm^{-1}) vs. pCFC-12 age (year) for water masses discussed in the present study (Table 1), with the surface layer omitted, as in Fig. 8.

and deep waters of the North Atlantic, values of a^*_{cdom} are generally higher than they are in the upper 500 m (Figs. 11(B) and (D)). The mean value of a^*_{cdom} within the AABW was the highest within the ocean interior (~0.27 m^2 g^{-1}, Fig. 11(A)) but this value was not as high as values found on the continental shelves. A plot of a^*_{cdom} vs. pCFC-12 derived age (Fig. 12(B)) shows a curve with a consistent increase in a^*_{cdom} with increasing ventilation age, with the exception of the upper (seasonal) thermocline layer (UTCL), which has a mean ventilation age similar to the surface layer (zero-age points were excluded from this analysis) but a much higher a^*_{cdom}.

4.4. Diagenesis of CDOM

The present hydrographic data set available from the CLIVAR Repeat Hydrography program allows us to quantitatively assess changes in the optical and chemical characteristics of the CDOM pool and how these changes occur relative to DOC. The dominant transformation of CDOM abundances we observed was the presumed bleaching of CDOM in the surface layer of the stratified subtropical central gyre. Bleaching dramatically reduced the absorption coefficient of CDOM in the SURF of the subtropical gyres (Figs. 6(A) and (C)) and also reduced the DOC-specific absorption coefficient a^*_{cdom} (Fig. 11(A) and (C)). This pattern reflects one of two things: either bleaching of CDOM is not necessarily equivalent to photooxidation of DOC to inorganic carbon species (Nelson et al., 1998, Del Vecchio and Blough, 2004) or the amount of DOC in the CDOM fraction is so small that significant photooxidation of CDOM chromophores does not affect DOC concentration in a measurable way (Nelson and Siegel 2002).

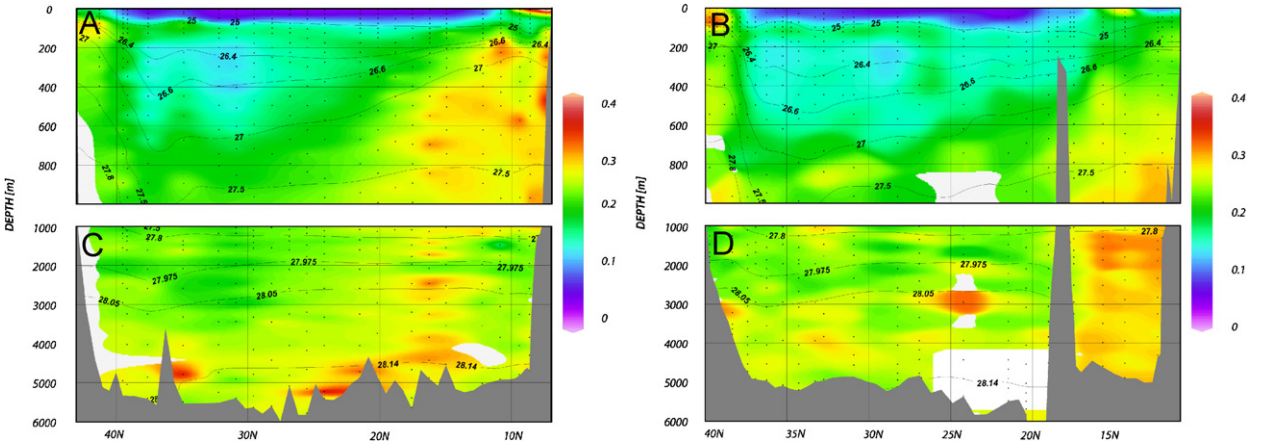

Fig. 11. Distribution of a^*_{cdom} ($m^2\,g^{-1}$), the DOC-specific absorption coefficient of CDOM at 325 nm along the A20 (A) and A22 (B) sections overlaid with neutral density contours, as in Figs. 3 and 6.

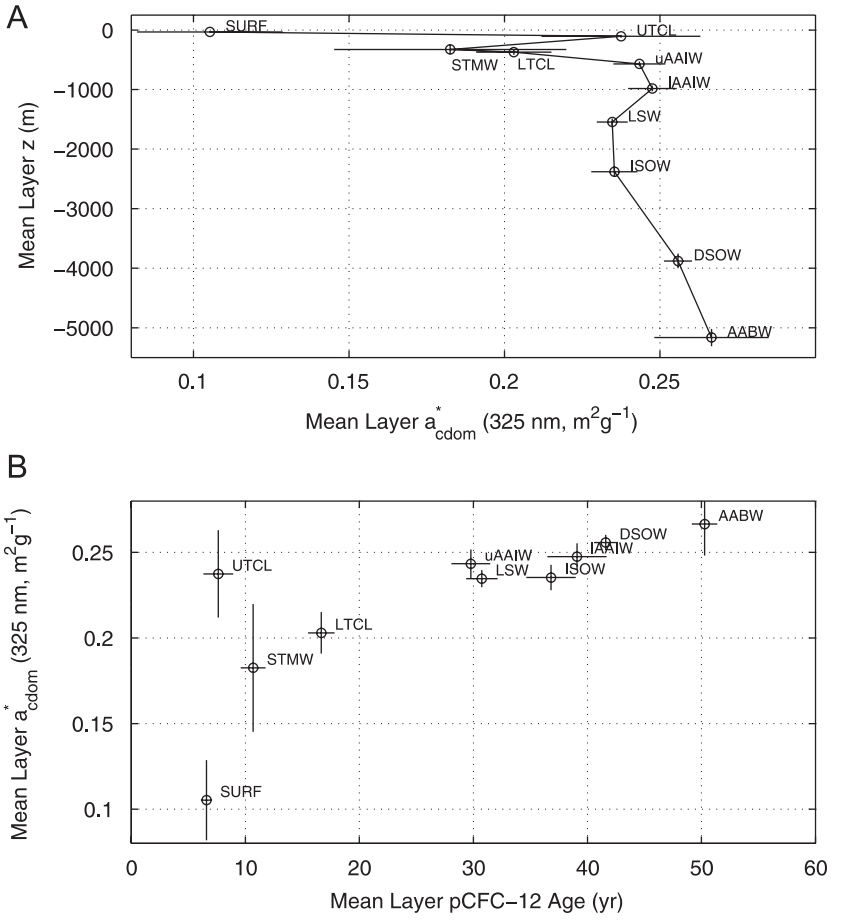

Fig. 12. (A) Mean depth profile for a^*_{cdom} ($m^2\,g^{-1}$) averaged within the various layers (Table 1). (B) Mean values of a^*_{cdom} ($m^2\,g^{-1}$) plotted vs. mean pCFC-12 age (year) within each layer.

We also observed increases in the spectral slope parameter S_{nlf} that correlated with decreases in a^*_{cdom} (Fig. 10 and Table 2). Our observations of reduced a^*_{cdom}, and increased S_{nlf} at the surface are consistent with trends observed in the Sargasso Sea (Nelson et al., 1998, 2004), on the North American

continental shelf (Vodacek et al., 1997), and in laboratory studies (Del Vecchio and Blough 2002). However, S_{nlf} values decreased with increasing age within each subsurface layer, with significant relationships found within most layers (Table 2), suggesting that low values of S_{nlf} found in the ocean can result from diagenesis of CDOM formed in situ in addition to indicating terrestrial-origin CDOM. When contrasted with the much less significant changes in CDOM abundance (Table 2), this pattern further suggests diagenesis of CDOM independent of quantity as assessed by absorption coefficient.

The pattern of changes in the value of a^*_{cdom} provides more clues about the diagenetic status of ocean CDOM stocks. The increase in a^*_{cdom} with increasing depth and age (Fig. 12), while mean CDOM not declining as much or significantly (Fig. 8, 9) suggests that CDOM in the deep ocean is more refractory than the DOC pool as a whole. The increase in a^*_{cdom} with increasing age (Fig. 12(B)) may be due to preferential remineralization of 'colorless' DOC, or preferential adsorption of colorless DOC onto particles (Druffel et al., 1998).

One further implication of these findings is that CDOM in the deep North Atlantic originates from SURF masses from higher latitudes that are not as bleached as subtropical SURF. Advection as viewed using the pCFC-12 age estimates appears to be fast enough to overcome in situ CDOM decomposition or in situ sources from other processes, such as the remineralization of the sinking rain of particulate organic carbon, except in the vicinity of the thermocline (Table 2), where a slow time increase of CDOM correlated with AOU suggests a weak local remineralization source.

4.5. Is CDOM a semi-conservative tracer?

We suggest from our analysis of the distribution of CDOM in the intermediate and deep waters of the central North Atlantic that CDOM is carried by the deep ocean circulation into the ocean interior, as is DOC (Hansell and Carlson, 1998). Furthermore, the relative homogeneity of CDOM in the deep North Atlantic suggests that advection and mixing dominate the distribution, and subsurface sources of CDOM are not as important. Intermediate waters show slow sources of CDOM in situ that presumably stem from remineralization sources (Coble et al., 1998, Nelson and Siegel, 2002). Can we nevertheless use CDOM as a passive tracer of ocean circulation?

One set of tests of this hypothesis is possible using the present data set. Portions of the OW component of the NADW (specifically the ISOW) were sampled on the A20 and A22 sections, but the source water is also found near its sill at ca. 2000 m along the A16N section near 60°N latitude. No significant trend in CDOM abundance (absorption coefficient at 325 nm) occurs in the ISOW (Fig. 8(E)), so we compare the mean CDOM abundance in the ISOW along the A20 and A22 sections ($0.1242\,m^{-1}$) to CDOM found within the neutral density surfaces delineating ISOW between 45°N and 60°N, where the water mass presumably passes through the A16N section ($0.1265\,m^{-1}$). The difference between these two means is within our presumed spectroscopic detection limit. We also extrapolated the value of the spectral slope parameter S_{nlf} back to time-zero using the regression of S_{nlf} vs. ventilation age (Table 2). The mean value of S_{nlf} in the ISOW along the A16N line was $0.0251\,nm^{-1}$ (std dev. $= 0.0035\,nm^{-1}$), and the extrapolated time-zero S_{nlf} from A20 and A22 S_{nlf} vs. pCFC-12 age was $0.0235\,nm^{-1}$. These are not unambiguous tests as variances within the datasets are relatively large, but it is nonetheless encouraging.

These results suggest CDOM is in fact useful as a semi-conservative tracer within a deep ocean water mass. Furthermore, CDOM is present in analytical quantities everywhere in the deep ocean we have so far sampled, in contrast to anthropogenic tracers. Finally, CDOM is quantifiable from space (Siegel et al., 2002, 2005b) so a surface boundary condition can be imposed on any model thus developed. It remains to diagnose CDOM dynamics in the upper water column in the context of local production and bleaching (Nelson et al., 1998).

Acknowledgments

We acknowledge the support of NSF Chemical Oceanography (OCE-0241614) and NASA Ocean Biology and Biogeochemistry (NAG5-13277) to DAS, NBN, and CAC. We thank the Repeat Hydrography Program, Rik Wanninkhof and Rana Fine, for support. Jon Klamberg and Stu Goldberg provided essential assistance at sea and in the laboratory. Dennis Hansell's group did the DOC analysis for P16N. Paula Coble, Scott Doney, and an anonymous reviewer provided very helpful comments on the manuscript. Thanks also to Chief

Scientists John Bullister, John Toole, Terry Joyce, and the captains and crew of the R/Vs *Knorr* and *Ron Brown*. Alexey Mishonov and Wilf Gardner, TAMU, arranged collection and preparation of samples for us on A16N Leg 1. W. Smethie's contribution was supported by NSF Grant OCE-0223951. LDEO contribution number 7027.

References

Alfutis, M.A., Cornillon, P., 2001. Annual and interannual changes in the North Atlantic STMW layer properties. Journal of Physical Oceanography 31, 2066–2086.

Arrigo, K.R., Brown, C.W., 1996. The impact of chromophoric dissolved organic matter on UV inhibition of primary productivity in the open ocean. Marine Ecology Progress Series 140, 207–216.

Blough, N.V., Zafiriou, O.C., Bonilla, J., 1993. Optical absorption spectra of waters from the Orinoco river outflow—terrestrial input of colored organic matter to the Caribbean. Journal of Geophysical Research 98, 2271–2278.

Boss, E., Zaneveld, J.R.V., 1993. The effect of bottom substrate on inherent optical properties: evidence of biogeochemical processes. Limnology and Oceanography 48, 346–354.

Byrne, R., Kaltenbacher, E., 2001. Use of liquid core waveguides for long pathlength absorbance spectroscopy: principles and practice. Limnology and Oceanography 46, 740–742.

Carder, K.L., Steward, R.G., Harvey, G.R., Ortner, P.B., 1989. Marine humic and fulvic acids: their effects on remote sensing of ocean chlorophyll. Limnology and Oceanography 34, 68–81.

Carlson, C.A., Giovannoni, S.J., Hansell, D.A., Goldberg, S.J., Parsons, R., Vergin, K., 2004. Interactions between DOC, microbial processes, and community structure in the mesopelagic zone of the northwestern Sargasso Sea. Limnology and Oceanography 49, 1073–1083.

Chen, R.F., Bada, J.L., 1992. The fluorescence of dissolved organic matter in seawater. Marine Chemistry 37, 191–221.

Chen, R.F., Bada, J.L., 1994. The fluorescence of dissolved organic matter in porewaters of marine sediments. Marine Chemistry 45, 31–42.

Coble, P.G., Del Castillo, C.E., Avril, B., 1998. Distribution and optical properties of CDOM in the Arabian Sea during the 1995 Southwest Monsoon. Deep-Sea Research Part II 45, 2195–2223.

Conmy, R.N., Coble, P.G., Chen, R.F., Gardner, G.B., 2004. Optical properties of colored dissolved organic matter in the Northern Gulf of Mexico. Marine Chemistry 89, 127–144.

D'Sa, E.J.R., Steward, G., Vodacek, A., Blough, N.V., Phinney, D., 1999. Optical absorption of seawater colored dissolved organic matter determined using a liquid capillary waveguide. Limnology and Oceanography 44, 1142–1148.

Del Castillo, C.E., Coble, P.G., Morell, J.M., Lopez, J.M., Corredor, J.E., 1999. Analysis of the optical properties of the Orinoco River plume by absorption and fluorescence spectroscopy. Marine Chemistry 66, 35–51.

Del Vecchio, R., Blough, N.V., 2002. Spatial and seasonal distribution of chromophoric dissolved organic matter and dissolved organic carbon in the Middle Atlantic Bight. Marine Chemistry 89, 169–187.

Del Vecchio, R., Blough, N.V., 2004. On the origin of the optical properties of humic substances. Environmental Science and Technology 38, 3885–3891.

Del Vecchio, R., Subramaniam, A., 2004. Influence of the Amazon River on the surface optical properties of the western tropical North Atlantic Ocean. Journal of Geophysical Research 109, C11001.

Determann, S., Reuter, R., Willkomm, R., 1996. Fluorescent matter in the eastern Atlantic Ocean. Part 2: vertical profiles and relation to water masses. Deep-Sea Research I 43, 345–360.

Doney, S.C., Jenkins, W.J., 1988. The effect of boundary conditions on tracer estimates of thermocline ventilation rates. Journal of Marine Research 46, 947–965.

Doney, S.C., Bullister, J.L., 1992. A chlorofluorocarbon section in the eastern North Atlantic. Deep-Sea Research 39, 1857–1883.

Doney, S.C., Jenkins, W.J., 1994. Ventilation of the Deep Western Boundary Current and Abyssal Western North Atlantic; Estimates from tritium and 3He distributions. Journal of Physical Oceanography 24, 638–659.

Doney, S.C., Jenkins, W.J., Bullister, J.L., 1997. A comparison of ocean tracer dating techniques on a meridional section in the eastern North Atlantic. Deep-Sea Research I 44, 603–626.

Druffel, E.R.M., Griffin, S., Bauer, J.E., Wolgast, D.M., Wang, X.C., 1998. Distribution of particulate organic carbon and radiocarbon in the water column from the upper slope to the abyssal NE Pacific ocean. Deep-Sea Research II 45, 667–687.

Feely, R.A., Talley, L.D., Johnson, G.C., Sabine, C.L., Wanninkhof, R., 2005. Repeat hydrography cruises reveal chemical changes in the North Atlantic. EOS Transactions of the American Geophysical Union 86 (399), 404–405.

Fine, R.A., Rhein, M., Andrie, C., 2002. Using a CFC effective age to estimate storage and propagation of climate anomalies in the deep western North Atlantic Ocean. Geophysical Research Letters 29, 2227.

Goldman, J.C., McCarthy, J.J., 1978. Steady state growth and ammonium uptake of a fast growing marine diatom. Limnology and Oceanography 23, 695–703.

Green, S.A., Blough, N.V., 1994. Optical absorption and fluorescence properties of chromophoric dissolved organic matter in natural waters. Limnology and Oceanography 39, 1903–1916.

Haine, T.W.N., Richards, K.J., 1995. The influence of the seasonal mixed layer on oceanic uptake of CFCs. Journal of Geophysical Research 100, 10727–10744.

Hall, M.M., Joyce, T.M., Pickart, R.S., Smethie Jr., W.M., Torres, D.J., 2004. Zonal circulation across 52°W in the North Atlantic. Journal of Geophysical Research 109, C11008.

Hansell, D.A., Carlson, C.A., 1998. Deep ocean gradients in the concentration of dissolved organic carbon. Nature 395, 263–266.

Hansell, D.A., 2002. DOC in the global ocean carbon cycle. In: Hansell, D.A., Carlson, C.A. (Eds.), Biogeochemistry of Marine Dissolved Organic Matter. Academic Press, San Diego, CA, pp. 685–715.

Højerslev, N., 1982. Yellow substance in the sea. In: Calkins, J. (Ed.), The Role of Solar Ultraviolet Radiation in Marine Ecosystems. Plenum Press, New York, pp. 263–281.

Jerlov, N.G., 1953. Influence of suspended and dissolved matter on the transparency of sea water. Tellus 5, 59–65.

Joyce, T.M., Deser, C., Spall, M.A., 2000. The relation between decadal variability of subtropical mode water and the North Atlantic Oscillation. Journal of Climate 13, 2550–2569.

Joyce, T.M., Pickart, R.S., Millard, R.C., 1999. Long-term hydrographic changes at 52 and 66°W in the North Atlantic Subtropical Gyre & Caribbean. Deep-Sea Research Part II 46, 245–278.

Joyce Jr., T.M., Hernandez-Guerra, A., Smethie, W.M., 2001. Zonal circulation in the NW Atlantic and Caribbean from a meridional World Ocean Circulation experiment hydrographic section at 66°W. Journal of Geophysical Research 106, 22095–22113.

Kalle, K., 1938. Zum problem der meerwasserfarbe. Annalen der hydrologischen und marinen mitteilungen 66, 1–13.

McGillicuddy, D.J., Johnson, R., Siegel, D.A., Michaels, A.F., Bates, N.R., Knap, A.H., 1999. Mesoscale variations of biogeochemical properties in the Sargasso Sea. Journal of Geophysical Research 104, 13381–13394.

McLachlan, J., 1964. Some considerations of the growth of marine algae in artificial media. Canadian Journal of Microbiology 10, 769–782.

McNeil, J.D., Jannasch, H.W., Dickey, T., McGillicuddy, D., Brzezinski, M., Sakamoto, C.M., 1999. New chemical, bio-optical and physical observations of upper ocean response to the passage of a mesoscale eddy off Bermuda. Journal of Geophysical Research 104, 15537–15548.

Miller, R.L., Belz, M., Del Castillo, C., Trzaska, R., 2002. Determining CDOM absorption spectra in diverse coastal environments using a multiple pathlength, liquid core waveguide system. Continental Shelf Research 22, 1301–1310.

Mopper, K., Zhou, X.L., Kieber, R.J., Kieber, D.J., Sikorski, R.J., Jones, R.D., 1991. Photochemical degradation of dissolved organic carbon and its impact on the oceanic carbon cycle. Nature 353, 60–62.

Nelson, N.B., Siegel, D.A., 2002. Chromophoric DOM in the open ocean. In: Hansell, D.A., Carlson, C.A. (Eds.), Biogeochemistry of Marine Dissolved Organic Matter. Academic Press, San Diego, CA, pp. 547–578.

Nelson, N.B., Siegel, D.A., Michaels, A.F., 1998. Seasonal dynamics of colored dissolved material in the Sargasso Sea. Deep-Sea Research I 45, 931–957.

Nelson, N.B., Carlson, C.A., Steinberg, D.K., 2004. Production of chromophoric dissolved organic matter by Sargasso Sea microbes. Marine Chemistry 89, 273–287.

Palter, J.B., Lozier, M.S., Barber, R.T., 2005. The effect of advection on the nutrient reservoir in the North Atlantic subtropical gyre. Nature 437, 687–692.

Pegau, W., Gray, D., Zaneveld, J.R.V., 1997. Absorption and attenuation of visible and near-infrared light in water: dependence on temperature and salinity. Applied Optics 36, 6035–6046.

Pickart, R.S., Smethie, W.M., Lazier, J.R.N., Jones, E.P., Jenkins, W.J., 1996. Eddies of newly formed Labrador Sea water. Journal of Geophysical Research 101, 20711–20726.

Prinn, R.G., Weiss, R.F., Fraser, P.J., Simmonds, P.G., Cunnold, D.M., Alyea, F.N., O'Doherty, S., Salameh, P., Miller, B.R., Huang, J., Wang, R.H.J., Hartley, D.E., Harth, C., Steele, L.P., Sturrock, G., Midgley, P.M., McCulloch, A., 2000. A history of chemically and radiatively important gases in air deduced from ALE/GAGE/AGAGE. Journal of Geophysical Research 105, 17751–17792.

Rhein, M., Fischer, J., Smethie, W.M., Smythe-Wright, D., Weiss, R.F., Mertens, C., Min, D.H., Fleischmann, U., Putzka, A., 1992. Labrador Sea Water: pathways, CFC inventory, and formation rates. Journal of Physical Oceanography 32, 648–665.

Schlitzer, R., 2004. Ocean Data View. 〈http://www.awi-bremerhaven.de/GEO/ODV/〉.

Siegel, D.A., Michaels, A.F., 1996. Quantification of non-algal light attenuation in the Sargasso Sea: implications for biogeochemistry and remote sensing. Deep-Sea Research II 43, 321–345.

Siegel, D.A., Maritorena, S., Nelson, N.B., Hansell, D.A., Lorenzi-Kayser, M., 2002. Global ocean distribution and dynamics of colored dissolved and detrital organic materials. Journal of Geophysical Research 107, 3228.

Siegel, D.A., Maritorena, S., Nelson, N.B., Behrenfeld, M.J., 2005a. Independence and interdependencies of global ocean color properties: reassessing the bio-optical assumption. Journal of Geophysical Research 110, C07011.

Siegel, D.A., Maritorena, S., Nelson, N.B., Behrenfeld, M.J., McClain, C.R., 2005b. Colored dissolved organic matter and the satellite-based characterization of the ocean biosphere. Geophysical Research Letters 32, L20605.

Smethie, W.M., Fine, R.A., 2001. Rates of North Atlantic deep water formation calculated from chlorofluorocarbon inventories. Deep-Sea Research I 48, 189–215.

Smethie, W.M., Fine, R.A., Putzka, A., Jones, E.P., 2000. Tracing the flow of North Atlantic deep water using chlorofluorocarbons. Journal of Geophysical Research 105, 14297–14323.

Steinberg, D.K., Nelson, N.B., Carlson, C.A., 2004. Production of chromophoric dissolved organic matter (CDOM) in the open ocean by zooplankton and the colonial cyanobacterium Trichodesmium spp. Marine Ecology Progress Series 267, 45–56.

Talley, L.D., Raymer, M.E., 1982. Eighteen degree water variability. Journal of Marine Research 40 (Suppl.), 757–777.

Toole, D.A., Siegel, D.A., 2004. Light-driven cycling of dimethylsulfide (DMS) in the Sargasso Sea: closing the loop. Geophysical Research Letters 31, L09308.

Twardowski, M.S., Boss, E., Sullivan, J.M., Donaghay, P.L., 2004. Modeling the spectral shape of absorption by chromophoric dissolved organic matter. Marine Chemistry 89, 69–88.

Vodacek, A., Blough, N.V., DeGrandpre, M.D., Peltzer, E.T., Nelson, R.K., 1997. Seasonal variation of CDOM and DOC in the Middle Atlantic Bight: terrestrial inputs and photooxidation. Limnology and Oceanography 42, 674–686.

Walker, S.J., Weiss, R.F., Salameh, P.K., 2000. Reconstructed histories of the annual mean atmospheric mole fractions for the halocarbons CFC-11, CFC-12, CFC-113, and carbon tetrachloride. Journal of Geophysical Research 105, 14285–14296.

Wallace, D.W.R., Lazier, J.R.N., 1988. Anthropogenic chlorofluoromethanes in newly formed Labrador Sea Water. Nature 332, 61–63.

Warner, M.J., Weiss, R.F., 1985. Solubilities of chlorofluorocarbons 11 and 12 in water and seawater. Deep-Sea Research Part II 32, 1485–1497.

Waugh, D.W., Haine, T.W.N., Hall, T.M., 2004. Transport times and anthropogenic carbon in the subpolar North Atlantic Ocean. Deep-Sea Research I 51, 1475–1491.

Worthington, L.V., 1959. The 18° water in the Sargasso Sea. Deep-Sea Research 5, 297–305.

Worthington, L.V., 1976. On the North Atlantic circulation, 1976. The Johns Hopkins Oceanography Study, vol. 6, 110pp.

Weiss, R.F., Bullister, J.L., Gammon, R.H., Warner, M.J., 1985. Nature 314, 608–610.

Yamashita, Y., Tanoue, E., 2004. In situ production of chromophoric dissolved organic matter in coastal environments. Geophysical Research Letters 31, L24302.

Zepp, R.G., Callaghan, T.V., Erickson, D.J., 1998. Effects of enhanced ultraviolet radiation on biogeochemical cycles. Journal of Photochemistry and Photobiology Part B: Biology 46, 69–82.